Sampathkumar *et al*. *Complex Eng Syst* 2024;4:3
DOI: 10.20517/ces.2023.34

Complex Engineering Systems

Research Article

Open Access

Fuzzy inference system-assisted human-aware navigation framework based on enhanced potential field

Shurendher Kumar Sampathkumar[1], Daegyun Choi[2], Donghoon Kim[2]

[1]Department of Mechanical and Materials Engineering, University of Cincinnati, Cincinnati, OH 45221, USA.
[2]Department of Aerospace Engineering and Engineering Mechanics, University of Cincinnati, Cincinnati, OH 45221, USA.

Correspondence to: Dr. Donghoon Kim, Department of Aerospace Engineering and Engineering Mechanics, University of Cincinnati, 2600 Clifton Ave, Cincinnati, OH 45221, USA. E-mail: Donghoon.Kim@uc.edu; ORCID: 0000-0003-3142-4458

How to cite this article: Sampathkumar SK, Choi D, Kim D. Fuzzy inference system-assisted human-aware navigation framework based on enhanced potential field. *Complex Eng Syst* 2024;4:3. http://dx.doi.org/10.20517/ces.2023.34

Received: 29 Sep 2023 **First Decision:** 24 Nov 2023 **Revised:** 9 Dec 2023 **Accepted:** 21 Dec 2023 **Published:** 13 Jan 2024

Academic Editor: Hamid Reza Karimi **Copy Editor:** Fangling Lan **Production Editor:** Fangling Lan

Abstract

With the advent of Autonomous Mobile Robots (AMRs) in public areas such as malls and airports, their harmonious coexistence with humans is crucial. AMRs must operate in a manner that ensures human safety, comfort, and acceptability to reduce stress. This is called Human Aware Navigation. This study introduces a framework for AMR navigation that prioritizes safety and human comfort in such environments, utilizing an enhanced Potential Field approach augmented by Fuzzy Inference Systems. To achieve a smooth AMR trajectory, the framework employs these systems based on AMR, human, and obstacle information. The proposed approach is tested across various scenarios, including complex, cluttered environments that mimic practical situations. Simulation results demonstrate that AMRs using the proposed method navigate human-rich environments safely and comfortably while mitigating common issues associated with Potential Field-based approaches, such as local minima and obstacles near the goal.

Keywords: Human Aware Navigation (HAN), Potential Field (PF), Fuzzy Inference System (FIS), Autonomous Mobile Robot (AMR)

1. INTRODUCTION

Asimov's first law of robotics [1] explicitly states that "A robot may not injure a human being or, through inaction, allow a human being to come to harm", serving as a foundational principle in human-robot interaction. While

this rule primarily concerns physical harm, the significance of safeguarding a person's psychological well-being cannot be understated. Currently, there is no established technology allowing robots to interpret the human mind, but research has been ongoing since the early 2000s to understand how robot actions may influence human psychological safety[2].

Traditionally, robots, especially Autonomous Mobile Robots (AMRs), have been utilized in factories and warehouses due to their efficiency in handling repetitive tasks[3]. However, recent years have witnessed the widespread deployment of AMRs in diverse settings, including restaurants[4,5], airports[6,7], and hospitals[3,8]. Surprisingly, despite the presence of humans in these environments, AMRs have often operated without due consideration for human safety. Nevertheless, some researchers[9,10] have concentrated on two generalized levels of safety: (i) physical safety, which involves avoiding collisions with humans; and (ii) psychological safety, which entails adhering to specific human norms, such as maintaining a safe distance from humans[9] and refraining from navigating certain areas near humans[10]. To mitigate the risk of collision with humans and alleviate human discomfort caused by AMRs' operation, proper navigation approaches for the AMRs are required.

In a typical AMR setup, the core components are often referred to as the "3P's", which play a critical role in its functionality[11]: Perception, Prediction, and Path planning. Here, perception represents mapping the AMR's surrounding environment, while prediction involves forecasting the future states of all the agents within that environment. Finally, path planning focuses on determining the safe course of action for the AMR to reach its next state. Scholars have frequently explored the interplay of these three components in the context of AMRs. For instance, Mateus *et al*. proposed a vision-based perception approach employing deep convoluted neural networks[12] for pedestrian detection. Their work featured a convolutional neural network-based aggregate channel features detector for pedestrian detection, alongside using asymmetric Gaussian functions to model human-aware constraints. The path planning was accomplished using the A* algorithm. Similarly, Bruckschen *et al*. delved into prediction, considering how humans navigate based on observations from the AMR and prior knowledge of human interactions with objects[13]. Hansen *et al*. developed an adaptive method for detecting a person's interest in interacting with the robot, relying on case-based reasoning and two-dimensional (2D) laser range measurements[14]. They further incorporated a time-dependent cost map for planning the AMR's path based on human future movement. In other works, such as the research by Ah *et al*.[15], a Probabilistic Road Map (PRM)-based algorithm was employed for the global path planner, while deep reinforcement learning was used for the local planner. The results obtained after evaluation with different environments and pedestrian behaviors exhibited improved AMR navigation with a reduced likelihood of colliding with humans.

In previous studies, it has become evident that the 3P's are intricately interconnected. However, the focus of this work predominantly centers on AMR's path planning, emphasizing the critical aspect of collision-free navigation while assuming the successful attainment of perception and prediction. In the domain of path planning research, diverse conditions and considerations have been employed by different researchers in designing their algorithms, encompassing aspects such as the nature of humans, algorithms, Human-Aware Navigation (HAN) models, and environmental factors. A summary of these variations is presented in Table 1.

The "nature of human" category relates to whether the human's position and heading exhibit changes over time. Meanwhile, the HAN model encompasses various constraints, including considerations such as respecting the human's intimate zone [Proxemics (PR)], avoiding navigation in the human's frontal space [Field of View (FV)], or refraining from traversing the area immediately behind the human [Back Space (BS)].

For instance, in the research conducted by Korkmaz *et al*., emphasis was placed on utilizing the A* algorithm as a primary planner, introducing a dynamic path planning method for HAN[16]. Their comparison between A* and PRM as navigation bases revealed that PRM could function as a quicker planner for HAN in comparison to A*. However, it often resulted in longer travel distances, steering the AMR away from humans. Notably, they

Table 1. Comparison of related works

Ref.	Nature of human	HAN model considered	Algorithm	Advantages	Disadvantages
[16]	Static	PR	PRM	Fast path planning compared to A*	Consideration of only static human and PR
[17]	Dynamic	PR	A*	Natural behavior of AMR, reduced planning time, time-dependent cost map	Consideration of PR only, planning timeout, computational burden
[18]	Dynamic	PR, FV	A*	Natural behavior of AMR, time-dependent cost map	Planning time-out, higher computational burden compared to [17]
[19]	Static	PR, FV, BS	APF	Smooth path compared to A*, no path planning timeout	Local minima and GNRON, consideration of only static human

did not consider that human moves over time and solely relied on PR. Moreover, the paths generated by both A* and PRM were found to be significantly influenced by the number of nodes [16,20]. Attempts to reduce the number of nodes in the A* map to alleviate computational burdens could compromise the path's smoothness. Similarly, Kirby *et al.* implemented a conventional A* path planner enhanced with social conventions, such as passing humans on the right [21]. Additionally, Kollmitz *et al.* designed a time-dependent deterministic planner using A*, which accounted for human motion [17]. However, this method solely relied on PR for navigation. They introduced a planning timeout within the algorithm, allowing it to stop after a fixed time and return the least-cost path to the destination. While this aids in timely algorithm termination, it occasionally yields sub-optimal paths or no path at all. Nonetheless, this algorithm ensures the AMR exhibits natural behaviors, such as avoiding close proximity to humans,

waiting for humans to pass, and adjusting its path in response to humans. Moreover, Briamonte *et al.* explored the application of the time-dependent deterministic A* path planning method for AMRs navigating in confined spaces around groups of humans, incorporating considerations of PR and FV [18]. However, their study observed longer navigation times compared to [17]. In another study by Sampathkumar *et al.*, the authors adopted the Artificial Potential Field (APF) for path planning, integrating human-associated factors through adjustable coefficients [19]. They optimized the path planning model using a genetic algorithm, fine-tuning coefficients such as scaling factors and Potential Field (PF) orders to minimize the AMR's path length while adhering to human-prescribed rules. Despite these improvements, their APF-based approach still encountered challenges related to local minima and difficulties reaching goals due to nearby obstacles, termed as goal non-reachable with obstacle nearby (GNRON) issues [22]. In short, the aforementioned studies include some level of limitations, such as a lack of consideration of sufficient human factors or human movement, planning timeout, or navigation issues (local minima and GNRON).

In light of these considerations, this work employs Enhanced PF (EPF) [23] as the foundational path planning technique. Furthermore, three human factors (PR, BS, and FV) are considered in this study, along with no planning timeout. The integration of EPF with HAN effectively addresses the limitations of APF while adhering to the principles of HAN in the AMR navigation. Additionally, the coefficients of EPF highly govern the behavior of AMRs. Hence, this research incorporates a Fuzzy Inference System (FIS) to dynamically adjust the coefficients within the HAN-EPF framework based on the system knowledge. This adaptive coefficient adjustment equips AMRs to effectively navigate within dynamically changing environments, accommodating the presence of humans with PR, BS, and FV considered human factors. The efficacy of the proposed approach is subsequently evaluated based on the AMR's ability to navigate to its destination while strictly adhering to HAN constraints, ensuring proper human-robot interaction and safety.

Overall, the main contributions of this work are

- To design a diverse human factors-employed HAN framework based on EPF that effectively overcomes local minima and GNRON issues.
- To employ the FISs to adaptively determine coefficients that enable the AMR to safely navigate in a dynam-

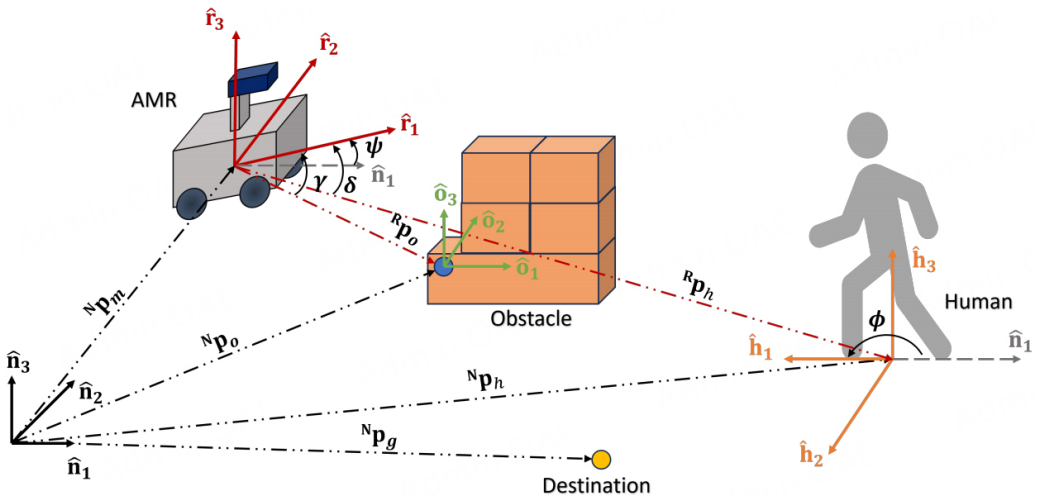

Figure 1. Definition of frames representation of vectors.

ically changing human-rich environment.

The paper is structured as follows: Section 2 lays the groundwork by defining frames and providing a concise overview of the EPF and FISs. Section 3 elaborates on the integration of HAN principles into the EPF framework and outlines the design of the FISs. In Section 4, the authors present and explore simulation results aimed at validating the performance of the proposed approach. Finally, Section 5 offers concluding remarks on this work.

2. PRELIMINARIES

2.1. Definition of frames and states

To describe the motion of the AMR, the reference frames, as shown in Figure 1, are established. The inertial frame is represented by $\hat{\mathbf{n}}_k$ for $k = 1, 2,$ and 3. The AMR's body frame is denoted by $\hat{\mathbf{r}}_k$, with its origin centered on the center of mass of the AMR's body. The AMR's primary movement direction aligns with $\hat{\mathbf{r}}_1$, while $\hat{\mathbf{r}}_3$ coincides with $\hat{\mathbf{n}}_3$. Accordingly, $\hat{\mathbf{r}}_2$ is determined using the right-hand rule. Similarly, the human's body frame is defined through $\hat{\mathbf{h}}_k$, with its origin situated at the center of mass of the human. Similar to the AMR's body frame, the forward direction of the human corresponds to $\hat{\mathbf{h}}_1$, and $\hat{\mathbf{h}}_3$ aligns with $\hat{\mathbf{n}}_3$. It is important to note that, given that the AMR generally lacks translational motion along $\hat{\mathbf{n}}_3$ and rotational motion along $\hat{\mathbf{n}}_1$ and $\hat{\mathbf{n}}_2$, this study adopts a 2D position vector and accounts for a rotational component about $\hat{\mathbf{n}}_3$.

The positions of the AMR, human, obstacle, and the AMR's destination in the inertial frame are denoted as ${}^N\mathbf{p}_m \in \mathbb{R}^2$, ${}^N\mathbf{p}_h \in \mathbb{R}^2$, ${}^N\mathbf{p}_o \in \mathbb{R}^2$, and ${}^N\mathbf{p}_g \in \mathbb{R}^2$, respectively. Here, the superscripts N, R, and H denote that the vector is represented in the inertial, AMR's body, and human's body frames, respectively. Note that the position vectors for the human and obstacle expressed in the AMR frame are described as

$$ {}^R\mathbf{p}_h = C_{RN}\, {}^N\mathbf{p}_h, \tag{1} $$

$$ {}^R\mathbf{p}_o = C_{RN}\, {}^N\mathbf{p}_o, \tag{2} $$

where C_{RN} represents the rotation matrix that maps from the inertial frame to the body frame, defined as

$$ C_{RN} = \begin{bmatrix} \cos\psi & \sin\psi \\ -\sin\psi & \cos\psi \end{bmatrix}. \tag{3} $$

Here, ψ represents the heading angle of the AMR, while the orientation of the human is denoted as ϕ. Also,

the relative angle between the AMR and the human in the AMR frame is expressed as δ, and the relative angle between the AMR and the obstacle within the AMR frame is defined as γ, as shown in Figure 1.

2.2. Enhanced potential field

The APF serves as a widely adopted method for robot collision avoidance owing to its mathematical efficiency and its capability to generate smooth obstacle-avoiding trajectories. This approach comprises two primary components: attraction and repulsion. An AMR is steered toward its destination by an attractive PF while being simultaneously pushed away from environmental obstacles through repulsive PFs. Consequently, a net PF emerges, which is the sum of both attractive and repulsive PFs, influencing the AMR's motion. The total potential function, denoted as Q_t governing the PFs, is defined as [23]

$$Q_t({}^N\mathbf{p}_m) = Q_a({}^N\mathbf{p}_m) + Q_r({}^N\mathbf{p}_M), \tag{4}$$

where

$$Q_a({}^N\mathbf{p}_m) = \frac{1}{2}k_a d({}^N\mathbf{p}_m, {}^N\mathbf{p}_g)^2, \tag{5}$$

$$Q_r({}^N\mathbf{p}_M) = \begin{cases} \frac{1}{2}k_r \left(\frac{1}{d({}^N\mathbf{p}_m, {}^N\mathbf{p}_o)} - \frac{1}{d_o}\right)^2 d({}^N\mathbf{p}_m, {}^N\mathbf{p}_g)^{n_g}, & \text{if } d({}^N\mathbf{p}_m, {}^N\mathbf{p}_o) \le d_o, \\ 0, & \text{if } d({}^N\mathbf{p}_m, {}^N\mathbf{p}_o) > d_o. \end{cases} \tag{6}$$

Here, $Q_a({}^N\mathbf{p}_m)$ is the attractive potential function, $Q_r({}^N\mathbf{p}_m)$ is the repulsive potential function, k_a and k_r are the attractive and repulsive coefficients, respectively, n_g is the potential order, $d(\mathbf{a}, \mathbf{b})$ is the distance between two generic position vectors $\mathbf{a}$ and $\mathbf{b}$, and d_o is the distance of influence. An essential improvement to note in the presented equation is the inclusion of an additional term $d({}^N\mathbf{p}_m, {}^N\mathbf{p}_g)^{n_g}$, which effectively addresses a well-known issue of the conventional APF known as GNRON [23]. Also, by taking the negative gradient of the respective terms, the total PF is derived as [23]

$$\mathbf{f}_t({}^N\mathbf{p}_m) = \mathbf{f}_a({}^N\mathbf{p}_m) + \mathbf{f}_r({}^N\mathbf{p}_m). \tag{7}$$

Note that the attractive and repulsive PFs are found by

$$\mathbf{f}_a({}^N\mathbf{p}_m) = -\nabla Q_a({}^N\mathbf{p}_m) = k_a d({}^N\mathbf{p}_m, {}^N\mathbf{p}_g) \frac{\partial d({}^N\mathbf{p}_m, {}^N\mathbf{p}_g)}{\partial\, {}^N\mathbf{p_m}}, \tag{8}$$

$$\mathbf{f}_r({}^N\mathbf{p}_m) = -\nabla Q_r({}^N\mathbf{p}_m) = \begin{cases} \mathbf{f}_{r_o}({}^N\mathbf{p}_m) + \mathbf{f}_{r_g}({}^N\mathbf{p}_m), & \text{if } d({}^N\mathbf{p}_m, {}^N\mathbf{p}_o) \le d_o, \\ 0, & \text{if } d({}^N\mathbf{p}_r, {}^N\mathbf{p}_o) > d_o, \end{cases} \tag{9}$$

where

$$\mathbf{f}_{r_o}({}^N\mathbf{p}_m) = -k_r \frac{d({}^N\mathbf{p}_m, {}^N\mathbf{p}_g)^{n_g}}{d({}^N\mathbf{p}_m, {}^N\mathbf{p}_o)^2} \left(\frac{1}{d({}^N\mathbf{p}_m, {}^N\mathbf{p}_o)} - \frac{1}{d_o}\right) \frac{\partial d({}^N\mathbf{p}_m, {}^N\mathbf{p}_o)}{\partial\, {}^N\mathbf{p_m}}, \tag{10}$$

$$\mathbf{f}_{r_g}({}^N\mathbf{p}_m) = -\frac{1}{2} n_g k_r d({}^N\mathbf{p}_m, {}^N\mathbf{p}_o)^{n_g - 1} \left(\frac{1}{d({}^N\mathbf{p}_m, {}^N\mathbf{p}_o)} - \frac{1}{d_o}\right)^2 \frac{\partial d({}^N\mathbf{p}_m, {}^N\mathbf{p}_g)}{\partial\, {}^N\mathbf{p_m}}. \tag{11}$$

Note that $\partial d({}^N\mathbf{p}_m, {}^N\mathbf{p}_g)/\partial\, {}^N\mathbf{p_m}$ is the direction from the AMR to the destination position, and $\partial d({}^N\mathbf{p}_m, {}^N\mathbf{p}_o)/\partial\, {}^N\mathbf{p_m}$ is the direction from the AMR to the obstacle. Nonetheless, a persistent challenge with the APF approach is

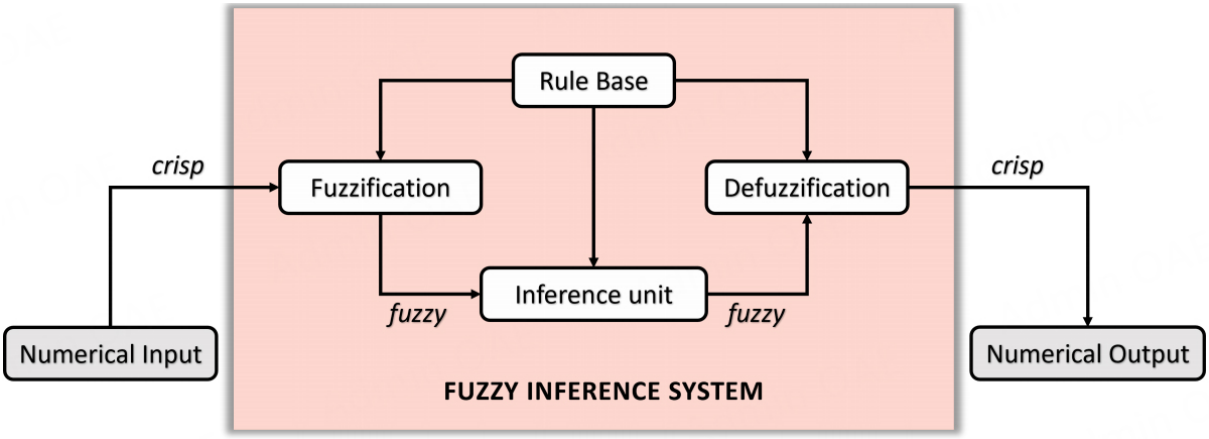

Figure 2. Schematic diagram of FIS.

the occurrence of local minima, particularly when one or more obstacles obstruct the AMR's path symmetrically. This issue stems from the criteria used to determine the direction of the repulsive PF. To mitigate this challenge, the following modification is introduced, replacing $\mathbf{f}_{r_o}({}^N\mathbf{p}_r)$ with a new term, as outlined in [23]:

$$\mathbf{f}_{r_e}({}^N\mathbf{p}_m) = -k_r \frac{d({}^N\mathbf{p}_m, {}^N\mathbf{p}_g)^{n_g}}{d({}^N\mathbf{p}_m, {}^N\mathbf{p}_o)^2} \left(\frac{1}{d({}^N\mathbf{p}_m, {}^N\mathbf{p}_o)} - \frac{1}{d_o} \right) \hat{\mathbf{q}}, \tag{12}$$

where $\hat{\mathbf{q}} \in \mathbb{R}^2$ is a newly defined repulsive PF direction vector given by

$$\hat{\mathbf{q}} = \frac{\mathbf{q}}{||\mathbf{q}||}, \tag{13}$$

where

$$\mathbf{q} = R_e({}^N\mathbf{p}_o - {}^N\mathbf{p}_m). \tag{14}$$

Note that $R_e \in \mathbb{R}^{2x2}$ is the rotation matrix given by

$$R_e = \begin{cases} R, & \text{if } \gamma < 0 \\ R^{\mathrm{T}}, & \text{if } \gamma \geq 0 \end{cases}, \tag{15}$$

where

$$R = \begin{bmatrix} \cos\theta & -\sin\theta \\ \sin\theta & \cos\theta \end{bmatrix}. \tag{16}$$

Here, θ represents a rotation angle responsible for altering the direction of the repulsive PF.

2.3. Fuzzy inference system

A FIS is an approach that employs a rule base and fuzzy set theory [24] to map inputs to outputs, as shown in Figure 2. When numerical data is input into the FIS, it undergoes a transformation into fuzzy inputs through fuzzification. This process involves assigning a degree of membership to each Membership Function (MF) corresponding to the numeric value. An MF precisely defines the degree to which an input value belongs to a fuzzy set. It maps input values from a precise domain onto a scale of the degree of membership, mostly ranging between 0 and 1. This scale indicates how strongly an element is associated with the set, allowing for a smooth transition between membership and non-membership states. Subsequently, the inference unit derives outputs based on user-defined rules, typically expressed in linguistic form; for example, "*If* Input 1 is Category 1 *AND* Input 2 is Category 2, *then* Output is Category 3". These outputs are associated with varying degrees

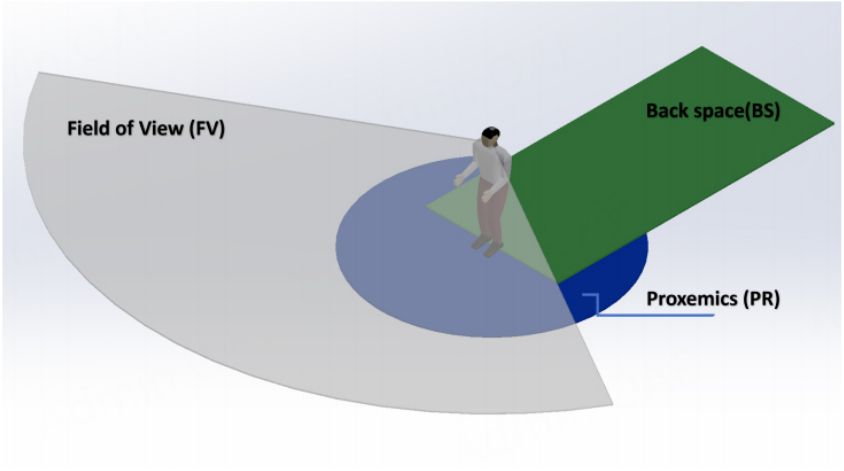

Figure 3. Representation of HAN factors with respect to a human.

of membership within output MFs. Finally, a process called defuzzification is employed to convert these fuzzy outputs back into numerical outputs. In this study, Mamdani-type FISs[24] are used and are referred to as FIS. One of the key advantages of FIS-based systems is their capacity to provide explainability, which can be attributed to the linguistically defined rules and MFs[25].

3. METHODOLOGY

3.1. Human aware navigation

HAN represents the convergence of robot motion planning and human-robot interactions[9]. While the primary aim of robot motion planning is to guide the robot to its destination, HAN prioritizes AMR's ability to minimize stress and prevent harm to humans. Therefore, it can be defined as "navigation of the AMRs based on human-centered PFs, aiming to minimize discomfort and prevent harm"[19].

Human discomfort stemming from AMRs can arise from various sources, including the robot's appearance, unnatural movement, production of discomforting noise, close proximity to humans, and failure to adhere to cultural norms[9]. Kruse *et al.* classified discomfort in HAN into three main categories: human comfort, AMR naturalness, and AMR sociability[9]. Human comfort revolves around ensuring maximum comfort and safety for humans in the presence of AMRs. Examples include AMRs maintaining a specified distance from humans at all times and refraining from traversing specific spaces near humans. AMR naturalness entails the robot's movement resembling that of humans, such as following smooth trajectories and having a friendly appearance, thereby enhancing acceptance. AMR sociability implies that the robot should adhere to cultural norms, such as traveling on a specific side (left/right) of humans depending on the country and overtaking humans along a certain direction. Among these categories, this work primarily focuses on human comfort concerning AMR navigation, as the robot's appearance and noise levels are not significantly related to its navigation. Safety takes precedence in this context.

This study introduces three important terms in HAN: PR, FV, and BS, as shown in Figure 3. PR signifies that the AMR must not only maintain a predetermined relative distance from humans at all times but also avoid collisions with them. BS denotes the region behind the human, where the presence of the AMR may cause discomfort to humans when traversing. FV represents the region in front of the human where the AMR could potentially obstruct the human's path. Consequently, a successful HAN planner must ensure that the AMR avoids these defined regions.

3.2. Proposed approach: HAN-EPF

3.2.1 Definitions of HAN factors

The primary focus of this study centers on the integration of factors associated with humans into the navigation of the AMR. To streamline collision-free path planning, it is assumed that the relative positions of humans with respect to the AMR are known, as this information can be obtained through optical or infrared sensors equipped with perception algorithms. Similarly, the relative position information of obstacles is obtained through lidar sensors. Note that obstacles are represented as a collection of points resembling cloud points. Data from the sensor, in the form of cloud points, is utilized to outline the boundaries of obstacles within the sensor's range. To account for HAN factors related to humans, this work introduces virtual cloud points surrounding a human. These virtual points are positioned along the perimeters of the HAN factors. To illustrate the formation of these virtual cloud points, Figure 4 depicts a parametric representation of the HAN factors in relation to a human, as introduced in the previous section.

The threshold distance for PR can vary considerably, depending on factors such as human age, the type of social interaction, and cultural norms[26]. However, in this work, PR is treated as a constant α_{PR} around the human center, in alignment with relevant studies[9,12,13]. Furthermore, the dimensions of the BS are defined using α_{BS_1} and α_{BS_2}, determined based on survey results[13]. Similarly, the angle and distance parameters for FV (α_{FV_1} and α_{FV_2}) are chosen considering the characteristics of human vision. Beyond a certain limit, known as the monocular vision area, human vision reduces to approximately one-fifth of normal human vision, leading to limited 3D perception and difficulty in viewing[27]. It is important to note that the generation of virtual cloud points for each HAN factor depends on the position and orientation of the human. Consequently, when the AMR detects a human within its sensing range, it generates virtual cloud points around the humans, taking into account the relevant HAN factors. These virtual cloud points for each HAN factor, as illustrated in Figure 4, are compactly formulated as

$$\begin{bmatrix} f_x \\ f_y \end{bmatrix} = D_j \, \Omega_j, \tag{17}$$

where f_x and f_y are the x and y coordinates of the virtual cloud point, respectively, D_j encompasses the geometric formulations involving varying δ angle, and Ω_j contains the dimensional information for each HAN factor, denoted as j and covering PR, BS, and FV. Here, Ω_j for each j is defined as $\Omega_{PR} = \alpha_{PR}$, $\Omega_{BS} = \begin{bmatrix} \alpha_{BS_1} & 0.5\alpha_{BS_2} \end{bmatrix}^{\mathrm{T}}$, and $\Omega_{FV} = \alpha_{FV2}$, and D_j is defined as

$$D_{PR} = \begin{bmatrix} \cos\delta \\ \sin\delta \end{bmatrix} \text{ for } 0 \le \delta < 2\pi, \tag{18}$$

$$D_{BS} = \begin{cases} \begin{bmatrix} 0 & 0 \\ 0 & 0 \end{bmatrix}, & \text{if } \delta < \frac{\pi}{2} \text{ or } \delta > \frac{3\pi}{2}, \\ \begin{bmatrix} -\tan(\delta - \pi/2) & 1 \\ 0 & 0 \end{bmatrix}, & \text{if } \delta \ge \frac{\pi}{2} \text{ or } \delta < \frac{\pi}{2} + \tan^{-1}\left(\frac{\alpha_{BS_1}}{0.5\alpha_{BS_2}}\right), \\ \begin{bmatrix} \tan(\delta - \pi/2) & -1 \\ 0 & 0 \end{bmatrix}, & \text{if } \delta > \frac{3\pi}{2} - \tan^{-1}\left(\frac{\alpha_{BS_1}}{0.5\alpha_{BS_2}}\right) \text{ or } \delta \le \frac{3\pi}{2}, \\ \begin{bmatrix} 0 & 0 \\ -1 & 1/\tan(\delta - \pi/2) \end{bmatrix}, & \text{if } \delta \ge \frac{\pi}{2} + \tan^{-1}\left(\frac{\alpha_{BS_1}}{0.5\alpha_{BS_2}}\right) \text{ or } \delta \le \frac{3\pi}{2} - \tan^{-1}\left(\frac{\alpha_{BS_1}}{0.5\alpha_{BS_2}}\right), \end{cases} \tag{19}$$

$$D_{FV} = \begin{cases} \begin{bmatrix} \cos\delta & \sin\delta \\ 0 & 0 \end{bmatrix}, & \text{if } \delta \leq \frac{\alpha_{FV_1}}{2} \text{ or } \delta \geq 2\pi - \frac{\alpha_{FV_1}}{2}, \\ \begin{bmatrix} 0 & 0 \\ 0 & 0 \end{bmatrix}, & \text{if } \frac{\alpha_{FV_1}}{2} < \delta < 2\pi - \frac{\alpha_{FV_1}}{2}. \end{cases} \tag{20}$$

To generate a specific virtual cloud point within the FV region, denoted as (f_x, f_y), the parameters Ω_{FV} and D_{FV} are used. Likewise, virtual cloud points for PR and BS are obtained based on the relative angle between the human and the AMR in the AMR frame.

3.2.2 Formulation of HAN-EPF

To account for human comfort in the AMR's navigation, an additional repulsive PF term is incorporated into the total PF. Consequently, the total PF of the HAN-EPF is expressed as

$$\mathbf{f}_t({}^N\mathbf{p}_m) = \mathbf{f}_a({}^N\mathbf{p}_r) + \mathbf{f}_r({}^N\mathbf{p}_m) + \mathbf{f}_h({}^N\mathbf{p}_m), \tag{21}$$

where $\mathbf{f}_h({}^N\mathbf{p}_m)$ is the repulsive PF associated with humans, serving as an additional component. The definition of $\mathbf{f}_h({}^N\mathbf{p}_m)$ is as follows:

$$\mathbf{f}_h({}^N\mathbf{p}_m) = \mathbf{f}_{h_g}({}^N\mathbf{p}_m) + \mathbf{f}_{h_e}({}^N\mathbf{p}_m), \tag{22}$$

where

$$\mathbf{f}_{h_g}({}^N\mathbf{p}_m) = -\frac{1}{2} n_g k_h d({}^N\mathbf{p}_m, {}^N\mathbf{p}_f)^{n_g - 1} \left(\frac{1}{d({}^N\mathbf{p}_m, {}^N\mathbf{p}_f)} - \frac{1}{d_o} \right)^2 \frac{\partial d({}^N\mathbf{p}_m, {}^N\mathbf{p}_g)}{\partial\, {}^N\mathbf{p_m}}, \tag{23}$$

$$\mathbf{f}_{h_e}({}^N\mathbf{p}_m) = -k_h \frac{d({}^N\mathbf{p}_m, {}^N\mathbf{p}_g)^{n_g}}{d({}^N\mathbf{p}_m, {}^N\mathbf{p}_f)^2} \left(\frac{1}{d({}^N\mathbf{p}_m, {}^N\mathbf{p}_f)} - \frac{1}{d_o} \right) \hat{\mathbf{q}}. \tag{24}$$

It is important to note that, at any given time step, only the closest virtual cloud point related to human factors and the closest obstacle point are considered. For instance, in Figure 5, all the HAN factors are detected in the left figure. However, the AMR is closer to FV than PR and BS. Hence, only FV is considered when generating $\mathbf{f}_h({}^N\mathbf{p}_m)$. Similarly, the obstacle point that is closer to AMR is used to compute $\mathbf{f}_r$. In the right figure, only BS is considered among the HAN factors.

The HAN-EPF contains several unknown parameters, but the dominant factors influencing the AMR's collision avoidance behavior are the coefficients k_a, k_r, and k_h. As determining proper suitable scaling factors typically involves trial and error and is a time-consuming process, this study introduced new variables, specifically the scaling factors μ_r and μ_h, to reduce the number of parameters and analyze the AMR's behavior concerning changes in those parameters. These variables replace k_r and k_h and are defined as follows:

$$k_r = \frac{k_a}{\mu_r}, \tag{25}$$

$$k_h = \frac{k_a}{\mu_h}. \tag{26}$$

Note that k_r and k_h are only dependent on the scaling factors once k_a is fixed. In this work, the scaling factors μ_r and μ_h, along with the coefficient k_a, are determined through the FISs proposed.

3.3. Preliminary study for understanding HAN-EPF

Before designing the FISs for the scaling factors, it is crucial to gain insights into how these scaling factors influence the AMR's behavior. This foundational understanding is essential for creating the MFs and rules for

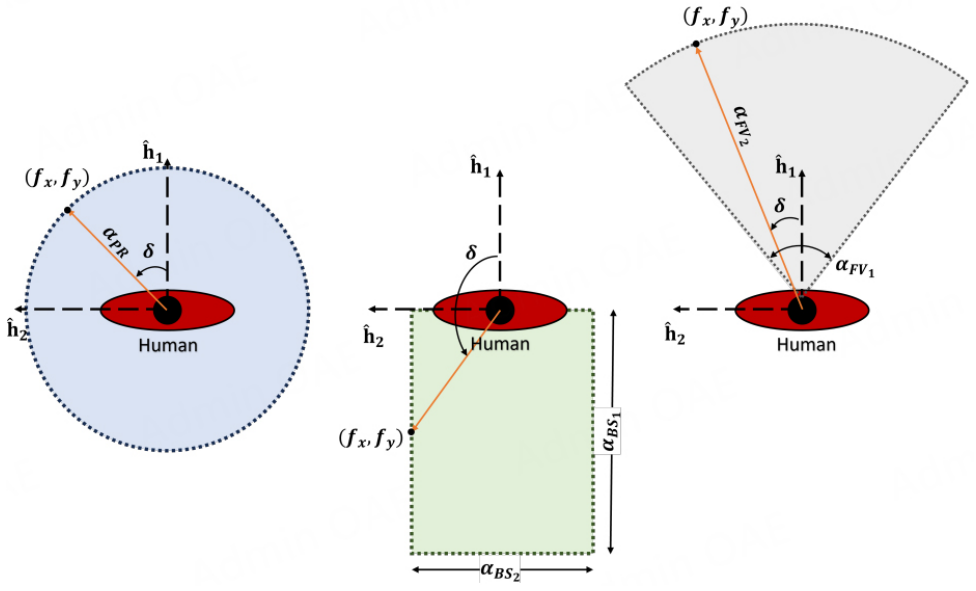

Figure 4. Virtual cloud points for each HAN factor (left - PR, middle - BS, right - FV).

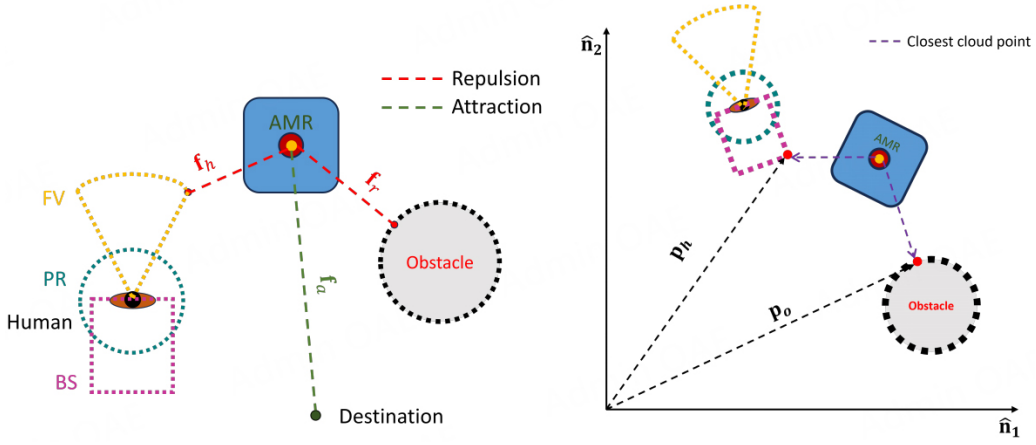

Figure 5. Illustrations for selecting HAN factors.

the proposed FISs. To achieve this, preliminary simulation studies were conducted to investigate the AMR's behavior in terms of its path length and relative distance from obstacles during avoidance maneuvers, with a focus on changes in the scaling factors. These preliminary results serve as the basis for designing the proposed FIS and help to establish reasonable ranges for the scaling factors. The simulation parameters introduced in Section 4 were utilized for these preliminary studies. Note that the coefficient k_a in the attractive PF was set to 1 to specifically observe how the AMR's behavior changes with varying μ_r values. The following observations were made from these preliminary studies. When the value of μ_r decreases beyond a certain value, the AMR's position starts to oscillate, as illustrated in Figure 6 (left). This oscillation occurs because the AMR traverses the boundary of the obstacle's distance of influence (d_o). On the other hand, increasing μ_r beyond a certain value causes the AMR to collide with the obstacle, as shown in Figure 6 (right). A threshold distance of 0.5 m was assumed to indicate a physical collision.

Due to the dominant attractive PF compared to the repulsive PF, the AMR is not effectively repelled from the obstacle. Consequently, when μ_r is high, the AMR travels closer to the obstacle, while a low μ_r results in a

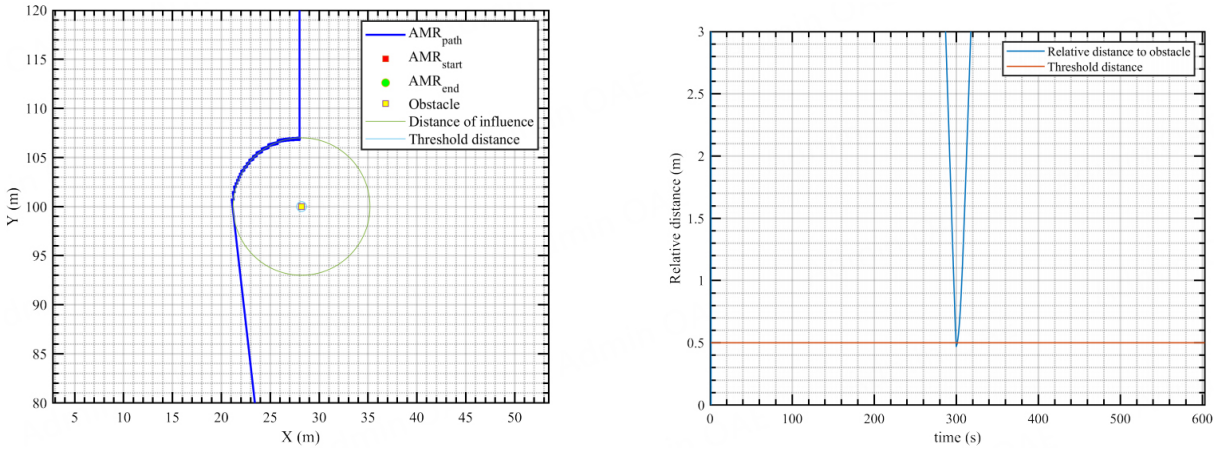

Figure 6. AMR's trajectory with very small μ_r (left) and relative distance between the AMR and the obstacle with very high μ_r (right).

longer path for the AMR, as shown in Figure 7.

It is noteworthy that the appropriate range for μ_r was found to be between 0.01 and 55, where neither collisions nor oscillations occurred. These preliminary simulations maintained k_a at 1 and the fixed distance of influence (d_o) at 25 m, reflecting typical lidar sensor sensing ranges. In addition, these analysis results can be applied to the scaling factor μ_h for humans, employing the same scaling factor range.

3.4. FIS design

This study employs three FISs to determine the coefficient k_a and scaling factors μ_r and μ_h. The first step in designing these FISs involves defining the appropriate inputs and outputs for each FIS. The structure of the FISs considered in this work is illustrated in Figure 8. For FIS 1, which determines the coefficient k_a (the output of the FIS 1), two inputs are selected: the relative distance between the AMR and the destination position and the relative distance between the AMR and either the obstacle or the human (whichever is closer). This choice is made because the magnitude of the attractive PF is closely tied to the AMR's motion toward the goal position. FIS 2 is responsible for determining the scaling factor μ_r, which governs the repulsive PF for obstacle avoidance. The inputs selected for FIS 2 include the relative distance of the AMR from the obstacle and the relative angle between the AMR's heading and the direction to the obstacle. These inputs are chosen to appropriately determine μ_r in relation to obstacle avoidance. FIS 3 derives the scaling factor μ_h, which is associated with interactions involving humans. The inputs for FIS 3 consist of the relative distance between the AMR and the human and the relative velocity of the AMR in relation to the human. These inputs are used to determine μ_h, which, in turn, influences the repulsive PF concerning human interactions.

For each input and output of the FISs, three MFs are considered, which are Low, Medium, and High. In particular, this work considers two sets of the MFs, as shown in Figure 9. The first set of the MFs in Figure 9 (left) is used for the inputs of all three FISs. These MFs normalize input numeric values within the range of 0 to 1. This normalization allows the FISs to be applicable across different environments and AMR velocities, provided that the maximum values are known. For FIS 1, the output uses the first set of MFs. On the other hand, the outputs of FIS 2 and FIS 3 use the second set of MFs defined in Figure 9 (right). The range of these output MFs, ranging from 0.01 to 55, is determined based on the preliminary studies described in the previous section.

The next step in designing the FISs is to build the rules that define the relationship between the inputs and outputs for each FIS, aiming to achieve the desired behavior of the AMR. As stated previously, FIS 1 determines the magnitude of the attractive PF. For example, if the AMR is in close proximity to obstacles or humans while

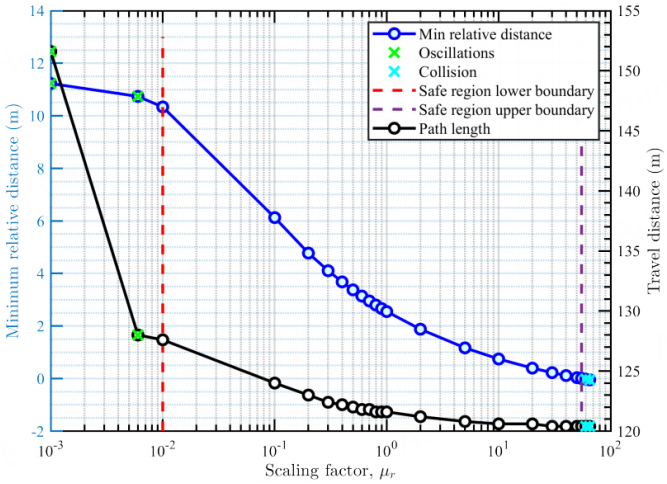

Figure 7. Minimum relative distance and the travel distance with respect to the scaling factor.

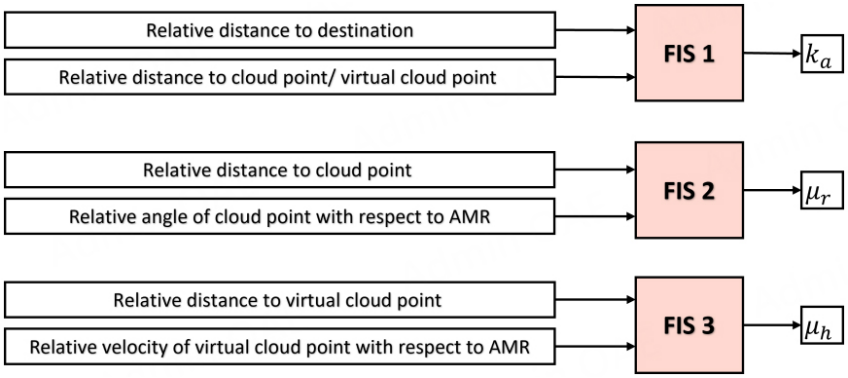

Figure 8. Structure of each FIS.

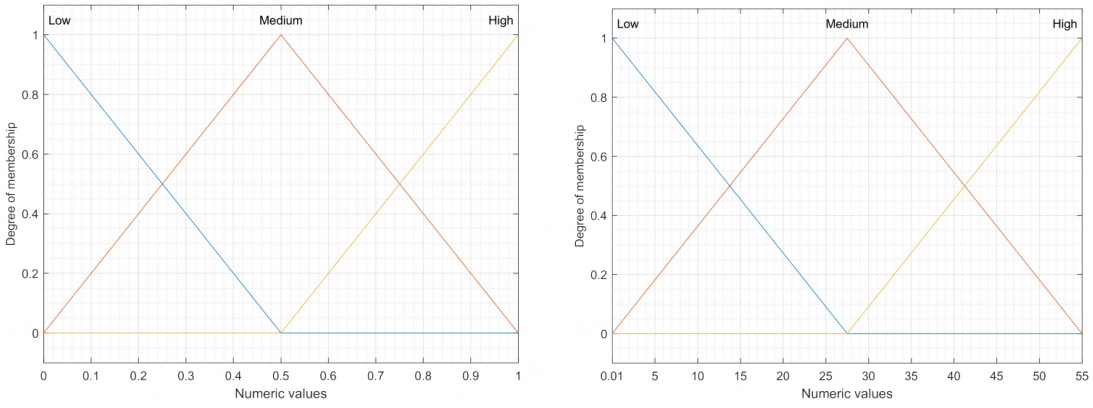

Figure 9. Two sets of the MFs considered.

being far from the goal position, it is desirable for the AMR to generate a smaller attractive PF than the repulsive one to avoid collisions, even if the relative distance to the goal is large. Conversely, if the AMR is far from both the destination and obstacles, it should generate a large attractive PF, which corresponds to a large value of k_a. Based on knowledge of the desired behavior of the AMR, the rules for FIS 1 are defined as shown in Table 2.

The next step in designing the FISs is to establish the rules for FIS 2, which determines μ_r and, consequently, k_r for the obstacle-associated repulsive PF. In contrast to FIS 1, FIS 2 takes into account the relative angle between the AMR and the obstacle. When the AMR is in close proximity to the obstacle and the relative angle is small, the AMR should generate a strong repulsive PF because a small relative angle indicates that the AMR is approaching the obstacle head-on. Consequently, μ_r should be set to "Low", resulting in a high value of k_r. The rules for FIS 2 are defined in Table 3 based on the desired avoidance maneuvers of the AMR.

Similar to FIS 2, FIS 3's rule matrix is designed to govern the desired avoidance maneuver of the AMR with respect to humans. For instance, when the AMR is in close proximity to a human and the relative velocity is high, a significant repulsive PF is needed. In such a case, where the human is approaching the AMR's direction, the AMR should have the capability to maneuver without violating HAN rules. This significant repulsive PF can be generated by setting μ_h to a small value. The rule matrix for FIS 3 is defined based on the AMR's motion concerning the input values, as shown in Table 4.

The entire process is summarized in the flowchart, as shown in Figure 10. Initially, once the parameters are defined, the human positional information is utilized to generate the virtual cloud points. Concurrently, the parameters used in the calculations concerning the AMR frame are inputted into the FIS to derive the outputs: k_a, μ_r, and μ_h. These resulting outputs, along with the virtual cloud points, are then fed into the EPF framework to calculate the total PF exerted on the AMR.

4. SIMULATION STUDIES

To validate the effectiveness and the performance of the proposed approach, simulation studies are performed, considering different environments using the parameters listed in Table 5.

To make the simulation realistic, the maximum human velocity is limited to 1.2 m/s, which is the preferred walking speed of humans [28]. In addition, in all scenarios, a threshold distance of 0.5 m is maintained between the AMR and obstacles or virtual cloud points. Crossing this threshold is considered a collision. This work considers three scenarios in the simulation studies. In Scenario 1, the AMR encounters three well-known issues sequentially: local minima, GNRON, and a moving human at distinct time steps. Scenario 2 takes into consideration a complex environment where the AMR encounters both obstacles and humans. Scenario 3 mimics a crowded real-life environment, such as an airport, where the AMR needs to navigate amidst many humans and obstacles, similar to a real-world infrastructure.

4.1. Scenario 1

In this scenario, the AMR maneuvers in an environment designed to introduce challenges such as local minima, GNRON, and the presence of a moving human. The environment includes a circular obstacle placed to block the AMR's head-on, causing a local minima issue, and a rectangular obstacle positioned near the destination position to create a GNRON issue. The parameters for the position information of the AMR and human are listed in Table 6.

Figure 11 (left) shows the AMR's trajectory in Scenario 1, demonstrating that the AMR adaptively avoids both the obstacle and the human during its travel. Also, Figure 11 (right) provides a visual representation of the scenario, highlighting that the AMR successfully maintains a relative distance greater than the collision threshold value of 0.5 m from both obstacles and the human. The closest relative distance between the AMR and the obstacle (purple dot) is 1.6 m, while the closest distance to the virtual cloud points (red dot) is 1.07 m. Furthermore, Figure 12 shows a close-up view of the AMR's interaction with the human. At 41 s, the AMR starts a maneuver when it encounters the human. Notably, the closest virtual cloud point corresponds to the FV, and based on the relative angle δ, the AMR navigates towards the back of the human. At 42 s and 44 s,

Table 2. Rule matrix for FIS 1

k_a		Relative distance to the goal		
		LOW	MEDIUM	HIGH
Relative distance to the obstacle	LOW	Medium	Medium	Low
	MEDIUM	Medium	Medium	High
	HIGH	High	High	High

Table 3. Rule matrix for FIS 2

μ_r		Relative distance to the obstacle		
		LOW	MEDIUM	HIGH
Relative angle to obstacle	LOW	Low	Low	Low
	MEDIUM	Low	Medium	Medium
	HIGH	High	High	High

Table 4. Rule matrix for FIS 3

μ_h		Relative distance to the virtual cloud point		
		LOW	MEDIUM	HIGH
Relative velocity to human	LOW	Low	Low	Low
	MEDIUM	Low	Medium	Medium
	HIGH	High	High	High

after navigating away from FV, the AMR successfully avoids PR and BS, respectively. Hence, throughout the simulation, the AMR reaches the destination position while avoiding the human and navigating safely without violating any HAN rules.

4.2. Scenario 2

Scenario 2 presents a more complex environment compared to Scenario 1, involving obstacles and moving humans. This environment consists of two humans, one in motion and the other rotating to change gaze, along with three obstacles. The parameters related to the positions of the AMR and human are given in Table 7.

Figure 13 displays the trajectory traveled by the AMR in Scenario 2. Despite facing two humans simultaneously near a static obstacle, the AMR adeptly navigates through this complex situation. Following this maneuver, the AMR safely reaches its destination while avoiding two static obstacles. Figure 13 (right) provides a visual representation of the relative distance between the AMR, obstacles, and humans. It can be observed that the closest relative distance between the AMR and the obstacles and the virtual cloud points are 1.15 and 1.06 m, respectively, both exceeding the collision threshold distance. Consequently, no collision occurs during the maneuver.

Figure 14 (top left) depicts the initial encounter between the AMR and human-1, who starts to rotate the AMR approaches. The AMR spends a significant portion of time navigating close to the FV of human-1, primarily because of the continuous rotation of their gaze. In response, the AMR adjusts its path, avoiding human-1 and subsequently encountering a rectangular obstacle near 58 s, as shown in Figure 14 (top right). When encountering the rectangular static obstacle, the robot prioritizes avoiding collision with it. Depending on the relative angle, the robot adjusts its navigation towards the right to circumvent the obstacle. Around 60 s, as shown in Figure 14 (bottom left), the AMR approaches a moving human and successfully navigates to the right side of the human, even though the human is moving toward the AMR. Note that the closest relative distance between the AMR and human-2 is highlighted by a red dot in Figure 13 (right), which occurs near the FV of human-2. Finally, at 70 s, as shown in Figure 14 (bottom right), the AMR bypasses human-2 and proceeds toward its destination, encountering both the rectangular obstacle and the circular obstacle along the way.

Table 5. Simulation parameters for the proposed HAN-EPF approach

Description	Value (unit)
Time interval, Δt	0.1 (s)
Order of potential, n_g	2
Distance of influence, d_o	25 (m)
Collision threshold distance	0.5 (m)
Repulsive field rotational angle, θ	45 (deg)
Sensing range	25 (m)
Maximum AMR velocity	1 (m/s)
Maximum human velocity	1.2 (m/s)
Proxemics range, α_{PR}	4 (m)
Back space range, α_{BS_1}	5 (m)
Back space width, α_{BS_2}	2.4 (m)
Field of view angle, α_{FV_1}	120 (deg)
Field of view range, α_{FV_2}	6 (m)

Table 6. Simulation parameters - Scenario 1

Description	Value (unit)
AMR start position	$\begin{bmatrix}90 & 160\end{bmatrix}^T$ (m)
AMR destination position	$\begin{bmatrix}90 & 40\end{bmatrix}^T$ (m)
Human start position	$\begin{bmatrix}47 & 34\end{bmatrix}^T$ (m)

Table 7. Simulation parameters - Scenario 2

Description	Value (unit)
AMR start position	$\begin{bmatrix}10 & 110\end{bmatrix}^T$ (m)
AMR destination position	$\begin{bmatrix}110 & 10\end{bmatrix}^T$ (m)
Human-1 start position	$\begin{bmatrix}38 & 79\end{bmatrix}^T$ (m)
Human-2 start position	$\begin{bmatrix}100 & 57\end{bmatrix}^T$ (m)

Table 8. Simulation parameters - Scenario 3

Description	Value (unit)
AMR start position	$\begin{bmatrix}20 & 10\end{bmatrix}^T$ (m)
AMR destination position	$\begin{bmatrix}5 & 65\end{bmatrix}^T$ (m)
Human-1 start position	$\begin{bmatrix}55 & 40\end{bmatrix}^T$ (m)
Human-2 start position	$\begin{bmatrix}60 & 70\end{bmatrix}^T$ (m)
Human-3 start position	$\begin{bmatrix}30 & 58\end{bmatrix}^T$ (m)
Human-4 start position	$\begin{bmatrix}12.5 & 5\end{bmatrix}^T$ (m)
Human-5 start position	$\begin{bmatrix}10 & 50\end{bmatrix}^T$ (m)
Human-6 start position	$\begin{bmatrix}62.5 & 15\end{bmatrix}^T$ (m)

Table 9. Closest relative distance from the AMR to humans and obstacles for each scenario

Scenario	Closest distance to human (m)	Closest distance to obstacles (m)
Scenario 1	1.07	1.6
Scenario 2	1.06	1.15
Scenario 3	0.55	0.89

4.3. Scenario 3

Scenario 3 considers a more realistic environment, resembling an airport setting with various humans and infrastructure-like obstacles. Circular obstacle-1 and circular obstacle-2 can be envisioned as pillars in an

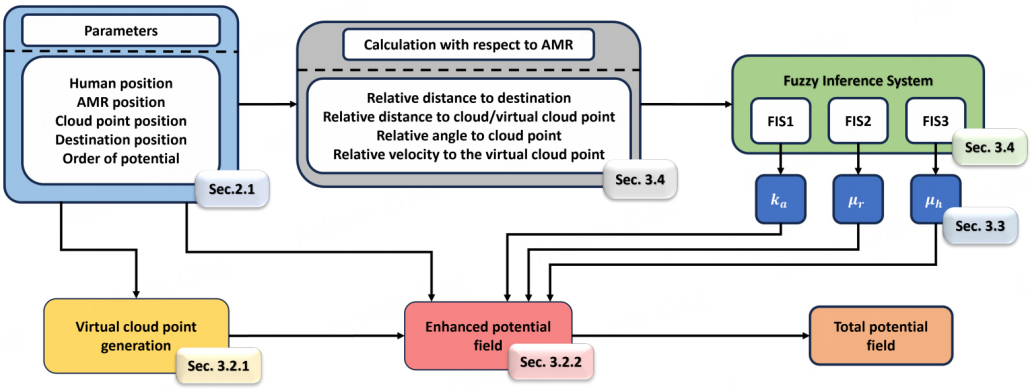

Figure 10. Overall procedure of the proposed approach.

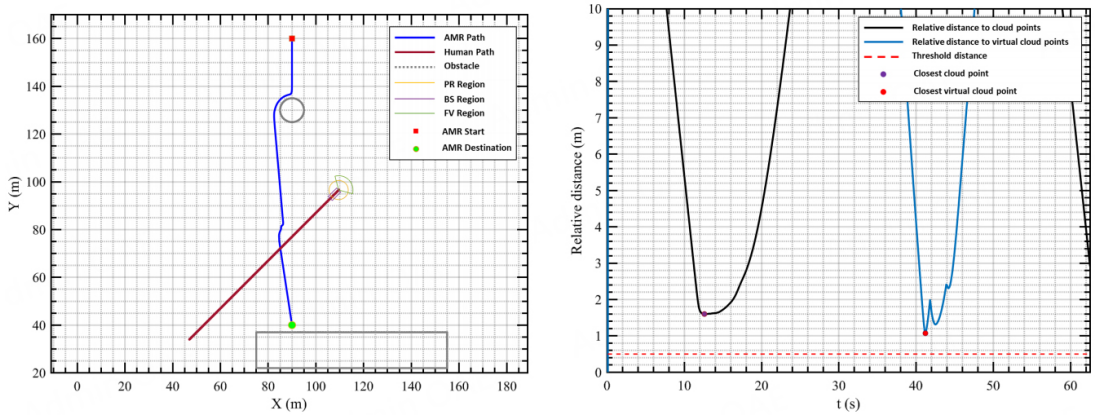

Figure 11. AMR's trajectory and relative distance from the AMR to obstacles and humans (Scenario 1).

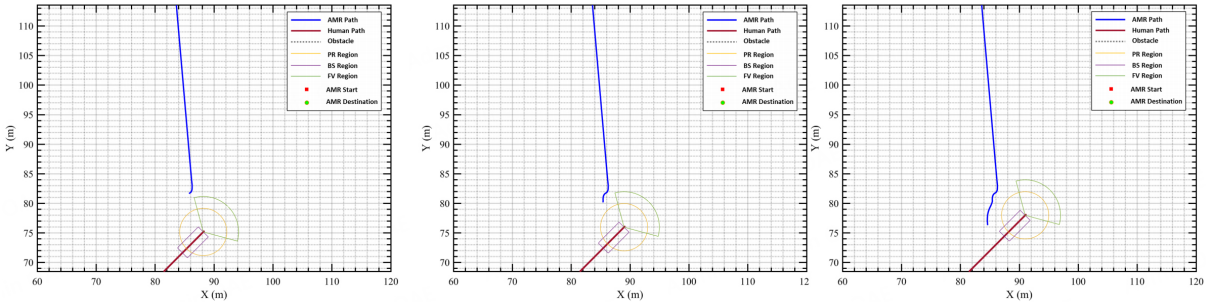

Figure 12. AMR's trajectories near humans (Scenario 1): (left) 41 s, (middle) 42 s, and (right) 44 s.

airport hallway, with humans following the convention of moving along the right side. In addition, there are two rectangular obstacles that represent passenger waiting regions. The simulation includes six human agents, and their positions are listed in Table 8.

From Figure 15 (right), one can observe that throughout the simulation, the AMR never crosses the collision threshold. The minimum relative distance between the AMR and obstacles, as well as the virtual cloud points around humans, are 0.89 m and 0.55 m, respectively. Figure 16 (top left) shows the initial encounter between the AMR and human-1, where the AMR maneuvers to the right at 10.5 s. However, it becomes evident that human-1 is moving faster than the AMR at 14.5 s, as shown in Figure 16 (top right). Consequently, the AMR

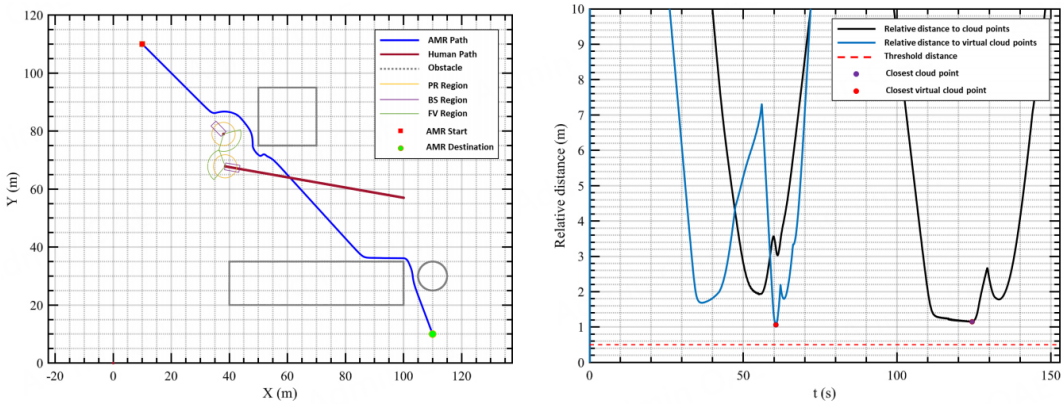

Figure 13. AMR's trajectory and relative distance from the AMR to obstacles and humans (Scenario 2).

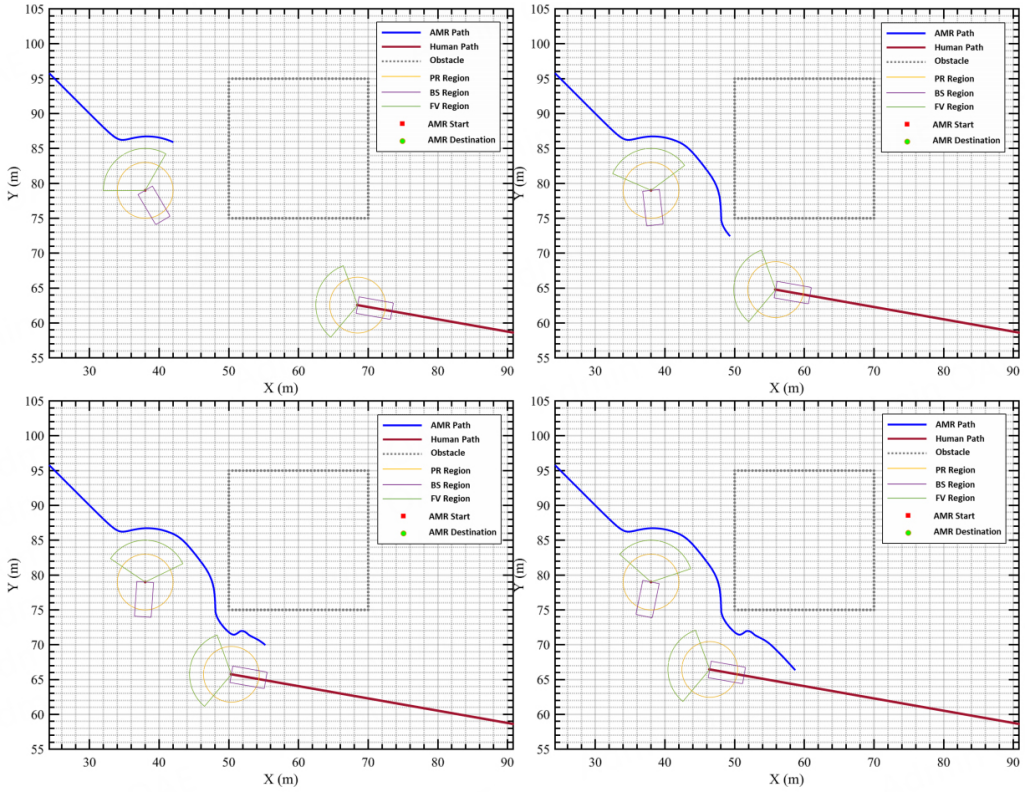

Figure 14. AMR's trajectories near obstacles and humans (Scenario 2): (top left) 42 s, (top right) 58 s, (bottom left) 65 s, and (bottom right) 70 s).

stops and maneuvers to the left to avoid a collision at 20 s, as shown in Figure 16 (middle left). Subsequently, the AMR prioritizes steering away from pillar-1 by choosing to navigate toward the left side. At around 35 s, the AMR faces human-2, who moves into its path and gazes in the AMR's direction, as shown in Figure 16 (middle right). The AMR successfully navigates the gap between FV of human-2 and the circular obstacle-1 during this maneuver, as depicted in Figure 16 (bottom left). Since the gap is small, the closest relative distance occurs during this maneuver of the AMR when the AMR encounters the FV of human-2. At 45 s, the AMR steers clear of human-2, as shown in Figure 16 (bottom left), and Figure 16 (bottom right) shows that at 65 s, it encounters human-3, who is moving in the same direction as the AMR but at a slower pace. Consequently, the AMR overtakes human-3 and reaches its destination. Note that human-4, located near the destination,

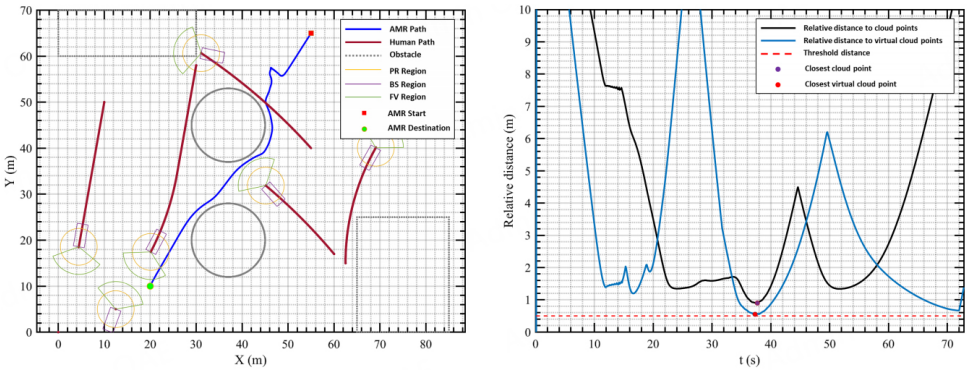

Figure 15. AMR's trajectory and relative distance from the AMR to obstacles and humans (Scenario 3).

presents a situation similar to GNRON.

To summarize the findings of the simulation study, the closest relative distances from the AMR to humans and obstacles obtained are tabulated in Table 9. Upon comparing various scenarios, it is observed that the relative distance from the AMR to humans is smaller than the distance from the AMR to obstacles. Since humans are moving, unlike static obstacles, during the operation of the AMR, there is a high possibility that the AMR navigates around humans closely. Furthermore, it is observed that the AMR comes closest to both humans and obstacles in Scenario 3 compared to the others. These results are natural as the AMR must navigate in a complex environment, dealing with dynamically moving humans and multiple static obstacles. Despite these challenges, it is noteworthy that in all scenarios, the AMR adeptly navigates to the destination position without violating any HAN constraints.

5. CONCLUSIONS

In this study, the authors introduce a HAN approach for AMRs through the integration of an EPF framework, referred to as HAN-EPF. The HAN-EPF method is designed by incorporating a repulsive PF that considers the impact of social constraints on human comfort during navigation. The concept of virtual cloud points is introduced when the AMR detects a human presence, effectively addressing these social constraints and ensuring safe and respectful interactions with humans. To simplify parameter selection, the coefficients of the repulsive PF are redefined in terms of the coefficient of the attractive PF and analyzed based on minimum relative distances and travel distances. Three FISs are employed to adaptively determine these redefined coefficients, guided by the design of MFs and rules based on analysis results. The approach's validation through simulation studies in diverse scenarios demonstrates effective AMR navigation, adherence to HAN rules, and avoidance of collisions with obstacles. Summarizing the important contributions of this work:

- Introducing the EPF as a foundational method for path planning, considering human factors, specifically PR, BS, and FV.
- Designing the FISs for the determination of the EPF's coefficients, assisting the AMR in successfully navigating in a human-populated environment that undergoes continuous changes.

In the future, the integration of a global planner alongside HAN-EPF as a local planner will be considered. This exploration involves testing this combined setup in environments characterized by an increased number of static obstacles.

Additionally, future plans involve delving into parameter optimization for the developed FISs using learning capabilities offered by optimization algorithms to achieve optimal routes for AMRs while adhering to the principles of the HAN framework.

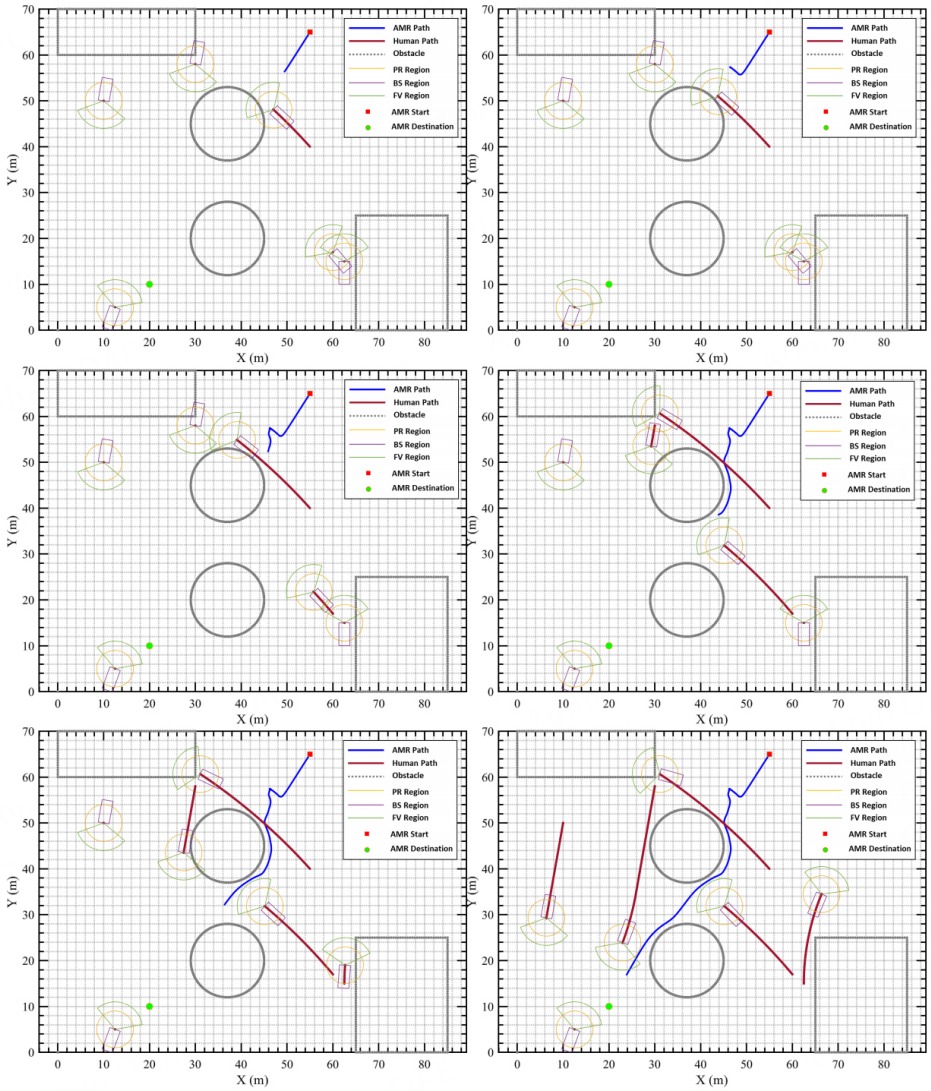

Figure 16. AMR's trajectories near obstacles and humans (Scenario 3): (top left) 10.5 s, (top right) 14.5 s, (middle left) 20 s, (middle right) 35 s, (bottom left) 45 s, and (bottom right) 65 s.

DECLARATIONS

Authors' contributions

Made substantial contributions to the conceptualization, methodology, and analysis: Sampathkumar SK, Choi D, Kim D

Contributed to approach validation, software simulation, and writing - original draft preparation: Sampathkumar SK, Choi D

Contributed to the investigation, supervision, and writing - review and preparation: Kim D

Availability of data and materials

Not applicable.

Financial support and sponsorship

None.

Conflicts of interest

All authors declared that there are no conflicts of interest.

Ethical approval and consent to participate

Not applicable.

Consent for publication

Not applicable.

Copyright

REFERENCES

1. Robertson N. The future of teaching? Asimov's three laws and the hypothetical robot teacher. *PRISM J* 2022;4:29-40. DOI
2. Butler JT, Agah A. Psychological effects of behavior patterns of a mobile personal robot. *Auton Robot* 2001;10:185-202. DOI
3. Fragapane G, Hvolby HH, Sgarbossa F, Strandhagen JO. Autonomous mobile robots in hospital logistics. In: IFIP international conference on advances in production management systems. Cham: Springer; 2020. pp. 672-79. DOI
4. Guo P, Shi H, Wang S, Tang L, Wang Z. An ROS architecture for autonomous mobile robots with UCAR platforms in smart restaurants. *Machines* 2022;10:844. DOI
5. Hasan OA, Alhakeem ZM, Armash MK, et al. Designing smart restaurant for reopening during the relaxation of lockdown in the time of corona pandemic. In: 2022 5th international conference on information and communications technology (ICOIACT), Yogyakarta, Indonesia; 2022. pp. 301-6. DOI
6. Wang J, Meng MQH. Path planning for nonholonomic multiple mobile robot system with applications to robotic autonomous luggage trolley collection at airports. In: 2020 IEEE/RSJ international conference on intelligent robots and systems (IROS), Las Vegas, NV, USA; 2020. pp. 2726-33. DOI
7. Tran HT, Vo TC, Nguyen QNA, et al. A novel design of a smart interactive guiding robot for busy airports. *Int J Smart Sens Intell Syst* 2022;15. DOI
8. Cheng L, Zhao N, Wu K, Chen Z. The multi-trip autonomous mobile robot scheduling problem with time windows in a stochastic environment at smart hospitals. *Appl Sci* 2023;13:9879. DOI
9. Kruse T, Pandey AK, Alami R, Kirsch A. Human-aware robot navigation: a survey. *Robot Auton Syst* 2013;61:1726-43. DOI
10. Nonaka S, Inoue K, Arai T, Mae Y. Evaluation of human sense of security for coexisting robots using virtual reality - 1st report: evaluation of pick and place motion of humanoid robots. In: IEEE international conference on robotics and automation, New Orleans, LA, USA; 2004. pp. 2770-75. DOI
11. Xin L. Dynamic path planning of multiple mobile robots. 2007. pp. 1-140. Available from: http://scholarbank.nus.edu.sg/handle/10635/13405 [Last accessed on 27 Dec 2023].
12. Mateus A, Ribeiro D, Miraldo P, Nascimento JC. Efficient and robust pedestrian detection using deep learning for human-aware navigation. *Robot Auton Syst* 2019;113:23-37. DOI
13. Bruckschen L, Bungert K, Dengler N, Bennewitz M. Human-aware robot navigation by long-term movement prediction. In: 2020 IEEE/RSJ international conference on intelligent robots and systems (IROS), Las Vegas, NV, USA; 2020. pp. 11032-37. DOI
14. Hansen ST, Svenstrup M, Andersen HJ, Bak T. Adaptive human aware navigation based on motion pattern analysis. In: RO-MAN 2009-The 18th IEEE international symposium on robot and human interactive communication, Toyama, Japan; 2009. pp. 927-32. DOI
15. Ah Sen N, Carreno-Medrano P, Kulić D. Human-aware subgoal generation in crowded indoor environments. In: Lecture notes in computer science. Cham: Springer; 2022. pp. 50-60. DOI
16. Korkmaz M. Human-aware dynamic path planning. In: 2021 international conference on INnovations in intelligent sysTems and applications (INISTA), Kocaeli, Turkey; 2021. pp. 1-5. DOI
17. Kollmitz M, Hsiao K, Gaa J, Burgard W. Time dependent planning on a layered social cost map for human-aware robot navigation. In: 2015 European conference on mobile robots (ECMR), Lincoln, UK; 2015. pp. 1-6. DOI
18. Briamonte A. Human-aware robot navigation around groups in narrow spaces. 2020. pp. 1-80. Available from: http://kth.diva-portal.org/smash/record.jsf?pid=diva2%3A1470222&dswid=-8798 [Last accessed on 27 Dec 2023].
19. Sampathkumar SK, Chhabra A, Choi D, Kim D. Optimization of artificial potential field using genetic algorithm for human-aware navigation of autonomous mobile robots. In: North American fuzzy information processing society annual conference. Cham: Springer; 2023. pp. 160-71. DOI
20. Zhang Y, Li Ll, Lin HC, Ma Z, Zhao J. Development of path planning approach using improved A-star algorithm in AGV system. *J Int Technol* 2019;20:915-24. Available from: https://jit.ndhu.edu.tw/article/view/2069 [Last accessed on 27 Dec 2023].
21. Kirby R, Simmons R, Forlizzi J. COMPANION: a constraint-optimizing method for person-acceptable navigation. In: RO-MAN 2009 - The 18th IEEE international symposium on robot and human interactive communication, Toyama, Japan; 2009. pp. 607-12. DOI
22. Khatib O. Real-time obstacle avoidance for manipulators and mobile robots. *Int J Robot Res* 1986;5:90-8. DOI

23. Choi D, Kim D, Lee K. Enhanced potential field-based collision avoidance in cluttered three-dimensional urban environments. *Appl Sci* 2021;11:11003. DOI
24. Mamdani EH. Application of fuzzy algorithms for control of simple dynamic plant. *IET* 1974;121:1585–88. DOI
25. Choi D, Chhabra A, Kim D. Collision avoidance of unmanned aerial vehicles using fuzzy inference system-aided enhanced potential field. Reston, VA: AIAA; 2022. p. 0272. DOI
26. Rios-Martinez J, Spalanzani A, Laugier C. From proxemics theory to socially-aware navigation: a survey. *Int J Soc Robot* 2015;7:137-53. DOI
27. Wheelwright B, Sulai Y, Geng Y, et al. Field of view: not just a number. In: Digital optics for immersive displays, Strasbourg, France; 2018. DOI
28. Shaganan T, Liu R, Yuen C, et al. Follow a human using a mobile robot regardless of the walking speed. In: 2018 3rd international conference on advanced robotics and mechatronics (ICARM), Singapore; 2018. pp. 351-56. DOI